Optical Engineering

OpticalEngineering.SPIEDigitalLibrary.org

Short-exposure turbulence effects on the modulation transfer function of annular aperture optical systems

David H. Tofsted

SPIE.

David H. Tofsted, "Short-exposure turbulence effects on the modulation transfer function of annular aperture optical systems," *Opt. Eng.* **56**(1), 015105 (2017), doi: 10.1117/1.OE.56.1.015105.

Short-exposure turbulence effects on the modulation transfer function of annular aperture optical systems

David H. Tofsted*
U.S. Army Research Laboratory, ATTN: RDRL-CIE-D, White Sands Missile Range, New Mexico 88002-5501, United States

Abstract. The results of recent analytical work performed to characterize the short-exposure blurring effects of path integrated optical turbulence for annular aperture systems is described using the modulation transfer function. Results presented here extend the circular case to the annular aperture problem involving a circularly symmetric central obscuration associated with telescope optics secondary mirrors. To enable this extension, adjustments to procedures that compute the tilt-variance and phase-tilt correlation effects are described, and the results are illustrated. A four-dimensionally parameterized function of turbulence strength, diffraction influence, angular frequency, and fractional central obscuration is given. © *The Authors. Published by SPIE under a Creative Commons Attribution 3.0 Unported License. Distribution or reproduction of this work in whole or in part requires full attribution of the original publication, including its DOI.* [DOI: 10.1117/1.OE.56.1.015105]

Keywords: atmospheric turbulence; atmospheric optics; image formation theory; modulation transfer function.

Paper 161463 received Sep. 26, 2016; accepted for publication Dec. 19, 2016; published online Jan. 24, 2017.

1 Introduction

The standard theory for modeling atmospheric turbulence impacts in systems performance models[1–3] has been Fried's[4] short-exposure atmospheric modulation transfer function (MTF). Reanalysis of Fried's approach has shown that when diffraction influences on the phase structure function are included,[5] the tilt-phase (TP) correlation term is numerically evaluated,[6] and path-dependent turbulence strength variations are considered.[7] However, like the original Fried work, only circular aperture geometries have been considered. This omits a significant class of telescope optics involving a central obscuration produced by reflector optics' circularly symmetric secondary mirror. The current paper summarizes efforts to close that gap.

The closest parallel works in the area of optical turbulence effects on annular aperture systems appear to be limited.[8,9] However, these primarily considered the modeling of phase perturbation terms and not the full short-exposure MTF.

The extension of the theory to incorporate this additional effect involves the introduction of a free parameter, here designated as C, the ratio of the inner obscuration diameter, D_1, to the outer system aperture diameter, D_2, such that $0 \leq C < 1$. The limit $C = 0$ corresponds to the circular solution.

The revised theory is addressed in general in Sec. 2. Thereafter, individual components of the calculation are considered separately, including the revised system MTF, the tilt-variance calculation, and the TP correlation calculation technique.

2 Short-Exposure Turbulence Modulation Transfer Function

The short-exposure turbulence MTF (SEMTF), based on Fried's approach, evaluates the impact of statistically averaged phase and amplitude fluctuations on image quality produced by an optical system. The statistics of the turbulence field is characterized by the wave and phase structure functions, denoted by $\mathcal{D}(r)$ and $\mathcal{D}_\phi(r)$, respectively. To generate averaged tilt-removed effects, the angle-of-arrival linear phase is mathematically removed. The linear tilt effects are deemed to shift the position of the centroid of the arriving pattern of photons but to not affect image quality. Only the remaining higher order phase and amplitude perturbations produce blur, resulting in MTF degradation.

The engine for the calculations performed involves the Rytov approximation's (RA) single-scattering model. This method was compared to the reportedly more robust method of Charnotskii[10] in Ref. 6. That paper also discussed limits of the RA based on Dashen's criteria.[11] However, here, for completeness, this discussion will be continued in Sec. 6.

2.1 *Dimensionless Variables Used*

The general optical problem encountered is illustrated in Fig. 1. An extended source object plane to be imaged is positioned at $z = -L$. The signal emitted is an incoherent light source consisting of uncorrelated photons, some of which pass through the receiver aperture entrance pupil at $z = 0$. The aperture consists of an annular ring whose maximum diameter is D_2 and whose inner obscuration diameter is D_1. The light studied is monochromatic with wavelength λ and wavenumber $k = 2\pi/\lambda$, and it passes through an atmosphere characterized by turbulence strength parameter C_n^2 ($\mathrm{m}^{-2/3}$) that in this paper is independent of path position.

From these variables, we can define a set of dimensionless variables that parameterize the optical problem. First, $C = D_1/D_2$ characterizes the aperture geometry. Second, $Q = D_2/(\lambda L)^{1/2} = D_2/F$ parameterizes diffraction influences, where F is the Fresnel zone. Third, $X = D_2/r_o$ characterizes the turbulence strength, where r_o is Fried's coherence diameter, $r_o = 3.018(k^2 L C_n^2)^{-3/5}$. To avoid the ubiquitous 2.1 factor, variables $\rho_o = r_o/2.1$ (the coherence length) and

*Address all correspondence to: David H. Tofsted, E-mail: david.h.tofsted.civ@mail.mil

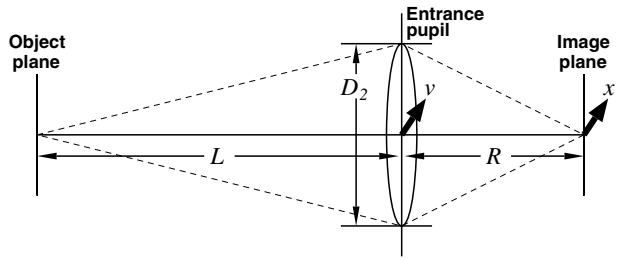

Fig. 1 Imaging geometry of the short-exposure imaging problem where optical turbulence fluctuations exist between the object plane and the system entrance pupil.

$S = D_2/\rho_o$ will also be used. This model ignores inner- and outer-scale of turbulence effects, whose impacts are minimal for incoherent imaging problems due to the mitigating factors of aperture averaging on the inner scale and aperture size ($D_2 < L_o$) on the outer scale. Impacts of path-varying turbulence were considered in Ref. 7.

The final governing variable is the dimensionless angular frequency ω, expressed in radians of frequency per radian of angle: Given a system aperture of outer diameter D_2 and wavelength λ, the maximum angular frequency is denoted $\Omega_o = D_2/\lambda$. This is the upper limit of variable $\Omega = Rf$ developed by Goodman[12] to aggregate the effects of the system focal length R and spatial frequency f in the system's image plane. Here, Goodman's Ω/Ω_0 is further reduced to the dimensionless frequency $\omega = \Omega/\Omega_o$, with limits $0 \le \omega \le 1$.

2.2 *Wave and Phase Structure Functions*

Let us next consider the form of the integrated wave and phase structure functions, given in terms of the above dimensionless parameters that describe the aggregate atmospheric turbulence properties. These functions were expressed in integral form for spherical wave propagation by Lawrence and Strohbehn[13]

$$\mathcal{D}(v) = \mathcal{D}_\ell(v) + \mathcal{D}_\phi(v) = 8\pi^2 k^2 L \int_0^1 \mathrm{d}c \int_0^\infty \mathrm{d}\kappa\kappa\Phi_n(\kappa)[1 - J_0(\kappa c v)], \tag{1}$$

for the wave structure function, and

$$\mathcal{D}_\phi(v) = 8\pi^2 k^2 L \int_0^1 \mathrm{d}c \int_0^\infty \mathrm{d}\kappa\kappa\Phi_n(\kappa)\,[1 - J_0(\kappa c v)]\cos^2 \times \left\{\kappa^2 \frac{c - c^2}{(2k/L)}\right\}, \tag{2}$$

for the phase structure function. Here, ℓ is a log-amplitude perturbation and ϕ is a phase perturbation at the system entrance pupil. $J_0(x)$ is the Bessel function of the first kind, order zero, and $c = (L + z)/L$ is a dimensionless path position, equal to zero at the object plane ($z = -L$) and unity at the system aperture ($z = 0$). The structure functions represent expectations of squared differences, e.g., $\mathcal{D}_\phi(v) = \langle[\phi(\mathbf{x}) - \phi(\mathbf{x} + \mathbf{v})]^2\rangle$.

The factor $\Phi_n(\kappa)$ is the refractive index power spectrum. In this analysis, a Kolmogorov spectrum is considered such that $\Phi_n(\kappa) = \beta C_n^2(z)\kappa^{-11/3}$, where $\beta \approx 0.033$ and κ (m^{-1}) is the spatial frequency of atmospheric turbulence fluctuations. Use of the Kolmogorov spectrum implies that the turbulence structure is homogeneous and isotropic. Note that the Bessel function terms involving J_0 produce a low frequency cutoff that further restricts outer scale influences.

The v variable in Eqs. (1) and (2) denotes a distance of spatial separation in a transverse plane between two observation points. In its truest sense, this variable must be treated as a vector quantity, but due to the choice of the isotropic/homogeneous Kolmogorov spectrum it loses its directional dependence. Hereafter, v will be a transverse distance measured in the system entrance pupil. In this case, it is also common to normalize v as a dimensionless variable (e.g., $u = v/D_2$) such that the above integrals can be reduced to the forms:[5]

$$\mathcal{D}(v, \rho_o) = \mathcal{D}(D_2 u, S = D_2/\rho_o) = 2(v/\rho_o)^{5/3} = [2(Su)^{5/3}] = J(Su), \tag{3}$$

and

$$\mathcal{D}_\phi(v, F, \rho_o) = J(Su)\alpha(Qu) = J(S/Q)[(Qu)^{5/3}\alpha(Qu)] = J(S/Q)Y(Qu). \tag{4}$$

Here, $\alpha(x)$ is a transitional function that varies between 1/2 at $x = 10^{-8}$, $\sim 3/4$ at $x = 10^{-1}$, and ~ 1 beyond about $x = 10$ (e.g., Fig. 1 of Ref. 5). In the numerical processing performed, this function is tabulated and interpolated as necessary. Also, $J(x)$ encapsulates the behavior of the wave structure function, while $Y(x)$ separates the u dependence of the phase structure function from the S dependence. This separation will be critical in Sec. 4's TP analysis.

The final form on the right side of Eq. (4) emphasizes that the turbulence-related S factor's influence has been decoupled from the u dependence in $Y(Qu)$. This will allow turbulence-related effects to be factored out of the integral in Eq. (50) of Sec. 4.

2.3 *Short-Exposure Turbulence Modulation Transfer Function Decomposition*

Given these preliminaries, the SEMTF can now be evaluated. In its compact form, the integral expression defining this function is given as[4,5]

$$M_S(\omega) = \frac{1}{A}\int \mathrm{d}\mathbf{v} W(\mathbf{v}) W(\mathbf{v} - D_2\boldsymbol{\omega}) \times \langle \exp\{\ell(\mathbf{v}) + \ell(\mathbf{v} - D_2\boldsymbol{\omega})\}\rangle \times \langle \exp\{i[\psi(\mathbf{v}) - \psi(\mathbf{v} - D_2\boldsymbol{\omega})]\}\rangle, \tag{5}$$

where $A = \pi D_2^2(1 - C^2)/4$ is the area of the system entrance pupil, $W(\mathbf{v})$ are window functions over this pupil, considered as binary functions (0 or 1), $\ell(\mathbf{v})$ is a propagated amplitude perturbation, and $\psi(\mathbf{v})$ is a tilt-corrected phase perturbation. The wavefront tilt over the aperture is characterized by $\mathbf{a}$, such that the tilt-corrected phase function in the system aperture can be expressed as $\psi(\mathbf{v}) = \phi(\mathbf{v}) - \mathbf{a} \cdot \mathbf{v}$. Fried[4] showed in detail that ℓ and ψ are independent random variables. Angle brackets are used to denote the expectation operator used to create the statistics for the net mean SEMTF.

The factor A imposes a normalization on the SEMTF integral: At zero frequency, $\boldsymbol{\omega} = 0$, we find that

$$M_S(0) = \frac{1}{A}\int \mathrm{d}\mathbf{v} W^2(\mathbf{v}) = 1. \tag{6}$$

This result also necessarily assumes $\langle \exp(2\ell)\rangle = 1$ [see, e.g., Equation (20) of Ref. 5. The principal difference between the short- and long-exposure imaging problems is the presence of ψ that replaces ϕ from the long-exposure case. The key element of the analysis of the SEMTF then reduces to the analysis of the expectation functions in Eq. (5). First, note that due to turbulence homogeneity, the relative starting point of these functions is indeterminate. Hence

$$\langle \exp\{\ell(\mathbf{v}) + \ell(\mathbf{v} - D_2\boldsymbol{\omega})\}\rangle \equiv \langle \exp\{\ell(0) + \ell(-D_2\boldsymbol{\omega})\}\rangle. \tag{7}$$

Also, because the turbulence is isotropic, the resulting functions will only depend on magnitude $D\omega$. We further define variables $\chi(u) = \ell(0) + \ell(D_2 u)$ and $\zeta(u) = \psi(0) - \psi(D_2 u)$. Prior analysis[4] showed that Eq. (5)'s expectations are expressible in terms of amplitude and tilt-corrected phase structure functions as

$$\langle \exp(\chi + i\zeta)\rangle = \exp\{-\mathcal{D}_\ell(v)/2 - \mathcal{D}_\psi(v)/2\}. \tag{8}$$

Variables χ and ζ are both Gaussian random variates that are independent of one another. Variable ζ is also a zero-mean quantity.

The annular aperture window function $W(\mathbf{v})$ can be constructed from a pair of functions $W_o(\mathbf{v}/D) = \mathrm{Cyl}(v/D)$ as

$$W(\mathbf{v}/D_2, C) = W_o(\mathbf{v}/D_2) - W_o[(\mathbf{v}/D_2)/C], \tag{9}$$

where $\mathrm{Cyl}(r) = 1$, if $r < 1/2$ and zero when $r \geq 1/2$. The open portion of the aperture integrates to $A = \pi D_2(1 - C^2)/4$. A normalized aperture ($D_2 = 1$) produces a normalized area $\hat{A} = \pi(1 - C^2)/4$.

Seemingly, the remaining step is to numerically evaluate the integrals with $\mathcal{D}_\ell(v)$ and $\mathcal{D}_\psi(v)$. However, upon decomposing $\mathcal{D}_\psi(D_2\boldsymbol{\omega})$, we find three terms

$$\begin{aligned}\mathcal{D}_\psi(D_2\boldsymbol{\omega}) &= \langle[\psi(\mathbf{v}) - \psi(\mathbf{v} - D_2\boldsymbol{\omega})]^2\rangle \\ &= \langle\{[\phi(\mathbf{v}) - \mathbf{a}\cdot\mathbf{v}] - [\phi(\mathbf{v} - D_2\boldsymbol{\omega}) - \mathbf{a}\cdot(\mathbf{v} - D_2\boldsymbol{\omega})]\}^2\rangle \\ &= \langle[\phi(\mathbf{v}) - \phi(\mathbf{v} - D_2\boldsymbol{\omega})]^2\rangle + \langle[\mathbf{a}\cdot(D_2\boldsymbol{\omega})]^2\rangle \\ &\quad - 2\langle[\phi(\mathbf{v}) - \phi(\mathbf{v} - D_2\boldsymbol{\omega})][\mathbf{a}\cdot(D_2\boldsymbol{\omega})]\rangle.\end{aligned} \tag{10}$$

To assess these components, note that the first term on the right is just the phase structure function, $\mathcal{D}_\phi(D_2\omega)$. Combining this term with the amplitude structure function of Eq. (8) yields a wave structure function. This combined term represents the long-exposure atmospheric turbulence MTF kernel. The remaining terms correspond to the short-exposure corrections. The first of these extra terms (center term on the right) is due to the tilt-variance. However, this term is positive in Eq. (10), which turns negative in Eq. (8), resulting in an overall degradation influence. Therefore, it is the final term on the right in Eq. (10), designated here as the TP correlation, that supplies the counteracting short-exposure correction to long-exposure turbulent blur.

The remaining task involves evaluating these remaining two terms, as well as assessing the net system MTF, defined as $M_0(\omega)$. To facilitate these computations, let us introduce a centered geometry

$$\begin{aligned}M_S(\omega) = \frac{1}{A}\int \mathrm{d}\mathbf{v} W(\mathbf{v}/D_2 + \boldsymbol{\omega}/2, C) W(\mathbf{v}/D_2 - \boldsymbol{\omega}/2, C) \\ \times \exp\{-\mathcal{D}(D_2\omega)/2 - \mathrm{TV} + \mathrm{TP}\},\end{aligned} \tag{11}$$

where TV is the tilt-variance term and TP is the tilt-phase correlation effect.

In the limit of negligible turbulence, the exponential term in Eq. (11) approaches unity, leaving the system MTF, $M_0(\omega, C)$, involving the integral of two shifted Eq. (9) window functions. The shifted overlapping windows are illustrated in Fig. 2. The frequency ω becomes the shift magnitude in the normalized aperture picture (D_2 becomes 1/2).

Function M_0 appears in integral form as

$$\begin{aligned}M_0(\omega, C) = \tilde{A}^{-1}\int \mathrm{d}\mathbf{u}\{W_o[\mathbf{u} + \boldsymbol{\omega}/2] - W_o[(\mathbf{u} + \boldsymbol{\omega}/2)/C]\} \\ \times \{W_o[\mathbf{u} - \boldsymbol{\omega}/2] - W_o[(\mathbf{u} - \boldsymbol{\omega}/2)/C]\},\end{aligned} \tag{12}$$

where $\mathbf{u} = \mathbf{v}/D_2$. To evaluate this integral, one must simply evaluate the areas of the two outer overlapping circles (the sum of areas S_1 through S_{10}) plus the overlapping inner circles (areas S_3 and S_4), then subtract off twice the overlap between an inner and an outer circle (e.g., areas S_1 through S_4). To evaluate these areas, consider a circle of radius R centered on the origin and integrated from $x = p$ ($-R \leq p \leq R$) through $x = R$. Let us write this result as

$$\begin{aligned}\tilde{U}(p, R) &= \int_p^R 2\sqrt{R^2 - x^2}\mathrm{d}x \\ &= R^2[\cos^{-1}(p/R) - (p/R)\sqrt{1 - (p/R)^2}] \\ &= R^2 U(p/R),\end{aligned} \tag{13}$$

where $-R \leq p \leq +R$. Using this result, for the overlapping outer circles, the net area is

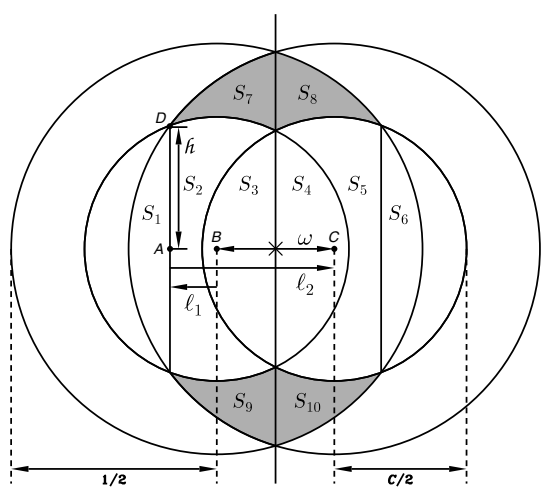

Fig. 2 Intersection of annular apertures displaced center-to-center from one another by amount ω of unit outer diameter and inner diameter $C = 9/14$. Subregions are labeled as S_1 through S_{10}. Cross marks center of coordinate system (origin of **v** vector space).

$$S_1 + \ldots + S_{10} = 2(1/2)^2 U[(\omega/2)/(1/2)] = U(\omega)/2. \tag{14}$$

The corresponding overlapping inner circle area is

$$S_3 + S_4 = 2(C/2)^2 U[(\omega/2)/(C/2)] = C^2 U(\omega/C)/2, \tag{15}$$

(assuming an overlap exists).

The overlap between inner and outer circles is also evaluated using the U function but requires that arguments ℓ_1 and ℓ_2 be determined. From Fig. 2, if rightward-directed arrows are considered positive valued, leftward arrows as negative valued, and ω as positive, then

$$\ell_1 + \ell_2 = \omega. \tag{16}$$

To evaluate ℓ_1 and ℓ_2, we also note that right triangles A-B-D and A-C-D share the common side of length h. Side B-D is $C/2$ long and side C-D is 1/2 long, leading to the following equations:

$$\ell_1^2 + h^2 = (C/2)^2 \quad \text{and} \quad \ell_2^2 + h^2 = (1/2)^2. \tag{17}$$

Subtracting these equations and using symbol $e = e(C) = (1 - C^2)/4$

$$\ell_2^2 - \ell_1^2 = e. \tag{18}$$

Equation (16) can be used to eliminate either ℓ_1 or ℓ_2 from Eq. (18), resulting in

$$\begin{aligned} \ell_1/R_1 &= K_1(\omega, C) = (\omega^2 - e)/(C\omega), \\ \ell_2/R_2 &= K_2(\omega, C) = (\omega^2 + e)/\omega. \end{aligned} \tag{19}$$

These results are directly comparable to the approach of Figs. 9–4 of Ref. 14. These expressions are just the arguments of the related U functions needed to evaluate these areas. Doubling the size of a single inner-outer overlapped area to account for S_1-S_4 plus S_3-S_6, produces the result

$$\mathcal{S}_{I/O}(\omega, C) = \left\{ \frac{U[K_2(\omega, C)] + C^2 U[K_1(\omega, C)]}{2} \right\} \times \left[\mathrm{Cyl}\left(\frac{\omega}{1+C}\right) - \mathrm{Cyl}\left(\frac{\omega}{1-C}\right) \right]. \tag{20}$$

Cylinder functions were added to handle the windowing of the function components. For shifts $\omega/2 < 1 - C$, the doubled inner circles lie completely inside the outer circles, whose net contributions are $2\pi C^2/4$. Combining normalized area terms and dividing by $\hat{A}$ yields the complete system MTF function, written as

$$\begin{aligned} M_0(\omega, C) &= \mathcal{G}_1(\omega, C) \\ &= \frac{2/\pi}{(1-C^2)} \left[U(\omega)\mathrm{Cyl}\left(\frac{\omega}{2}\right) + C^2 U(\omega/C)\mathrm{Cyl}\left(\frac{\omega}{2C}\right) \right] \\ &\quad - \frac{4/\pi}{(1-C^2)} \mathcal{S}_{I/O}(\omega, C) - \frac{2C^2}{(1-C^2)} \mathrm{Cyl}\left(\frac{\omega}{1-C}\right). \end{aligned} \tag{21}$$

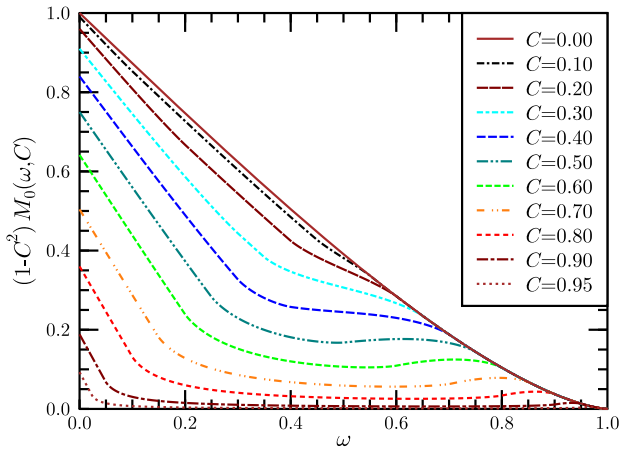

Fig. 3 Unnormalized annular aperture system MTF curves for the $C = D_1/D_2$ parameter ranging from 0.0 to 0.95.

Various versions of this function for different choices of parameter C are plotted in Fig. 3. While the basic function is normalized such that $M_0(0, C) = 1$, the curves plotted in Fig. 3 have been multiplied by $(1 - C^2)$ to preserve a sense of the relative entrance pupil in terms of its light-gathering capacity.

The next two sections cover the calculation of the tilt-variance (TV) term in Sec. 3 and the TP correlation term in Sec. 4.

3 Annular Aperture Tilt-Variance Calculations

In this section, we consider the TV term in Eq. (11). In general, the TV is found to be aperture geometry dependent, but because the turbulence is assumed isotropic and the apertures are circularly symmetric, the tilt statistics is also isotropic ($\langle \mathbf{a} \cdot \mathbf{a} \rangle = \langle a_x^2 \rangle + \langle a_y^2 \rangle = 2\langle a_x^2 \rangle = 2\langle a_y^2 \rangle$). Components a_x and a_y are also decorrelated ($\langle a_x a_y \rangle = 0$). Therefore, we can write

$$\begin{aligned} \mathrm{TV} &= \frac{1}{2} \langle [\mathbf{a} \cdot (D_2 \boldsymbol{\omega})]^2 \rangle = \frac{D_2^2}{2} \langle a_x^2 \omega_x^2 + 2 a_x a_y \omega_x \omega_y + a_y^2 \omega_y^2 \rangle \\ &= \frac{\langle \mathbf{a} \cdot \mathbf{a} \rangle}{4} (D_2^2 \omega^2). \end{aligned} \tag{22}$$

It remains to evaluate $\langle \mathbf{a} \cdot \mathbf{a} \rangle$. To do so, accounting for annular aperture influences, we return to an analysis of Fried's[15] phase perturbation model. The instantaneous phase perturbation function $\phi(\mathbf{v})$ can be decomposed into an infinite series of weighted orthonormal basis functions

$$\phi(\mathbf{v}) = \sum_{\mu=0}^{\infty} p_\mu F_\mu(\mathbf{v}). \tag{23}$$

This expression may also be dissected in the form

$$\phi(\mathbf{v}) = \sum_{\mu=0}^{N-1} p_\mu F_\mu(\mathbf{v}) + \sum_{\mu=N}^{\infty} p_\mu F_\mu(\mathbf{v}) = \Phi_N(\mathbf{v}) + \mathscr{H}_N(\mathbf{v}), \tag{24}$$

where the lower order terms are resolved and the higher order remainder, $\mathscr{H}_N$, is unresolved.

Fried ordered the F_μ basis functions such that the first few would involve the piston (index 0), tip (1), and tilt (2) terms, such that

$$\phi(\mathbf{v}) = \Phi_3(\mathbf{v}) + \mathscr{H}_3(\mathbf{v}); \quad \text{where } \Phi_3(\mathbf{v}) = p_0 F_0(\mathbf{v}) + p_x F_x(\mathbf{v}) + p_y F_y(\mathbf{v}). \tag{25}$$

Also, $\Phi_0 = 0$ (no expansion terms), such that $\mathscr{H}_0(\mathbf{v}) = \phi(\mathbf{v})$. In general, the total unresolved instantaneous phase variance averaged over the system aperture can be evaluated via the integral

$$\Delta_N^2 = \int d\mathbf{v} \frac{W(|\mathbf{v}|)}{A} \mathscr{H}_N^2(\mathbf{v}) = \int d\mathbf{v} \frac{W(|\mathbf{v}|)}{A} [\phi(\mathbf{v}) - \Phi_N(\mathbf{v})]^2 = \sum_{\mu=N}^{\infty} \frac{(p_\mu)^2}{A}. \tag{26}$$

In incoherent imaging, once a photon appears on the system image plane, knowledge of the mean phase is lost. Thus, the lowest order measureable phase error is Δ_1^2. Short-exposure imaging further reduces the phase error by eliminating tip and tilt effects since a centroid shift will not reduce point-source image quality. Hence, we focus on Δ_3^2. The difference, $\Delta_1^2 - \Delta_3^2 = (p_x^2 + p_y^2)/A$, is proportional to the TV.

Evaluating this difference involves calculating p_x and p_y coefficients based on integrations using the F_j basis functions. Fried required that these follow the normalization rule

$$\int d\mathbf{x} W(x) F_\mu(\mathbf{x}) F_\nu(\mathbf{x}) = \begin{cases} 1, & \mu = \nu; \\ 0, & \mu \neq \nu. \end{cases} \tag{27}$$

The piston, tip, and tilt terms are given by

$$F_0(\mathbf{v}) = \frac{1}{\sqrt{\pi(D_2^2 - D_1^2)/4}} = \frac{1}{A^{1/2}}, \tag{28}$$

$$F_1 = F_x(\mathbf{v}) = W_T v_x, \qquad F_2 = F_y(\mathbf{v}) = W_T v_y, \tag{29}$$

where $W_T = 8/[\pi D_2^4(1 - C^4)]^{1/2}$ has dimensions of inverse area. These factors yield orthonormal annular functions (see, e.g., Ref. 9) as opposed to Fried's circular aperture factors.

The expansion coefficients p_μ are then evaluated using

$$p_\mu = \int d\mathbf{x} W(|\mathbf{x}|) \phi(\mathbf{x}) F_\mu(\mathbf{x}). \tag{30}$$

Dimensionally speaking, the p_μ's are the lengths, the F_μ's are the inverse lengths, and their products are dimensionless. Fried's[4] $\mathbf{a} \cdot \mathbf{v}$ product was also dimensionless but used lengths for $\mathbf{v}$ and inverse lengths for $\mathbf{a}$, although their analogs F_μ and p_μ, respectively, were of opposing dimensional senses. The tilt vector components a_μ are therefore related to quantities p_μ as $a_\mu v_\mu = p_\mu F_\mu = (p_\mu W_T) v_m u$, such that

$$\langle \mathbf{a} \cdot \mathbf{a} \rangle = \langle W_T^2 (p_x^2 + p_y^2) \rangle = W_T^2 A \langle (\Delta_1^2 - \Delta_3^2) \rangle. \tag{31}$$

To evaluate $\Delta_1^1 - \Delta_3^2$, let us follow Fried's development. We first write this difference as

$$\Delta_1^2 - \Delta_3^2 = (\Delta_0^2 - \Delta_3^2) - (\Delta_0^2 - \Delta_1^2). \tag{32}$$

We then evaluate the two forms from Eq. (32) using the p_μ forms of Eqs. (30) in (26)

$$\begin{aligned} \Delta_0^2 - \Delta_N^2 &= \sum_{\mu=0}^{N-1} \frac{p_\mu^2}{A} \\ &= \frac{1}{A} \sum_{\mu=0}^{N-1} \left[\int d\mathbf{x} W(|\mathbf{x}|) \phi(\mathbf{x}) F_\mu(\mathbf{x}) \right] \left[\int d\mathbf{x}' W(|\mathbf{x}'|) \phi(\mathbf{x}') F_\mu(\mathbf{x}') \right] \\ &= \frac{1}{A} \int d\mathbf{x}' W(|\mathbf{x}|) \left[\sum_{\mu=0}^{N-1} \int d\mathbf{x}' W(|\mathbf{x}'|) F_\mu(\mathbf{x}) F_\mu(\mathbf{x}') \right] \phi(\mathbf{x}) \phi(\mathbf{x}'). \end{aligned} \tag{33}$$

Now, let us introduce Fried's[15] "trick" involving the rewriting of Δ_0^2 in a form resembling the bracketed final section of Eq. (33). First,

$$\begin{aligned} \Delta_0^2 &= \sum_{\mu=0}^{\infty} \frac{p_\mu^2}{A} = \int d\mathbf{x} \frac{W(|\mathbf{x}|)}{A} \phi^2(\mathbf{x}) \\ &= \int d\mathbf{x} \frac{W(|\mathbf{x}|)}{A} \left[\sum_{\mu=0}^{N-1} \int d\mathbf{x}' W(|\mathbf{x}'|) F_\mu(\mathbf{x}) F_\mu(\mathbf{x}') \right] \phi^2(\mathbf{x}). \end{aligned} \tag{34}$$

The trick involves recognizing that the bracketed region only produces a result for its $F_0(\mathbf{x})$ term in Eq. (34). All other components integrate to zero due to orthogonality. For the zeroth component, the integral evaluates to $A^{1/2}$, which cancels with $F_0 = A^{-1/2}$.

Symmetrizing Eq. (34) into the form,

$$\Delta_0^2 = \int d\mathbf{x} \frac{W(|\mathbf{x}|)}{A} \left[\sum_{\mu=0}^{N-1} \int d\mathbf{x}' W(|\mathbf{x}'|) F_\mu(\mathbf{x}) F_\mu(\mathbf{x}') \right] \times \left[\frac{\phi^2(\mathbf{x}) + \phi^2(\mathbf{x}')}{2} \right], \tag{35}$$

Equations (33) and (35) can be combined to write

$$\Delta_N^2 = \sum_{\mu=0}^{N-1} \int \frac{d\mathbf{x} W(|\mathbf{x}|)}{2A} \int d\mathbf{x}' W(|\mathbf{x}'|) F_\mu(\mathbf{x}) F_\mu(\mathbf{x}') [\phi(\mathbf{x}) - \phi(\mathbf{x}')]^2. \tag{36}$$

Taking the expectation of both sides

$$\langle \Delta_N^2 \rangle = \sum_{\mu=0}^{N-1} \int d\mathbf{x} \frac{W(|\mathbf{x}|)}{2A} \int d\mathbf{x}' W(|\mathbf{x}'|) F_\mu(\mathbf{x}) F_\mu(\mathbf{x}') \mathcal{D}_\phi(|\mathbf{x} - \mathbf{x}'|). \tag{37}$$

Next, vectors $\mathbf{x}$ and $\mathbf{x}'$ are replaced by $\mathbf{r} = \mathbf{x} - \mathbf{x}'$ and $\mathbf{s} = (\mathbf{x} + \mathbf{x}')/2$, permitting Eq. (37) to be written as

$$\langle \Delta_N^2 \rangle = \frac{\pi}{A} \int_0^{D_2} \mathcal{F}_N(r) \mathcal{D}_\phi(r) r dr, \tag{38}$$

using

$$\mathcal{F}_N(r)=\int \mathrm{d}\mathbf{s}W\left(\left|\mathbf{s}+\frac{\mathbf{r}}{2}\right|\right)W\left(\left|\mathbf{s}-\frac{\mathbf{r}}{2}\right|\right)\sum_{\mu=0}^{N-1}F_\mu\left(\mathbf{s}+\frac{\mathbf{r}}{2}\right)F_\mu\left(\mathbf{s}-\frac{\mathbf{r}}{2}\right). \tag{39}$$

Terms related to $\mathbf{s}$ can now be collected and integrated separately. Due to circular symmetry of the entrance pupil, the resulting functions depend only on magnitude $r = |\mathbf{r}|$. From this result, the tilt-variance becomes

$$\langle \mathbf{a}\cdot\mathbf{a}\rangle = D_2^2 W_T^2 \int_0^1 [\mathcal{G}_1(u,C)-\mathcal{G}_3(u,C)]\mathcal{D}_\phi(D_2 u)u\mathrm{d}u, \tag{40}$$

where the C parameter denotes the additional influence of the central obscuration and the $\mathcal{F}_\mu$ functions involving dimensional arguments v (m) have been converted to functions $\mathcal{G}_\mu$ featuring dimensionless spatial distances $u = r/D_2$.

At this point, given available space, just the results of further manipulations will be shown. Calculation details were discussed in Ref. 16.

For the circular aperture case, the tilt-variance can be written as

$$\langle \mathbf{a}\cdot\mathbf{a}\rangle = 2.0864 J(S)G(Q)/D_2^2, \tag{41}$$

where S measures the turbulence strength and $G(Q)$ gauges the relative effects of diffraction through parameter Q involving the transition from 0.5 for $Q < 1$ to 1.0 for $Q \geq 2$. It can be expressed approximately using the below equation:

$$G(Q) = \Sigma_P(\hat{q}, +0.908, +0.361, +0.092, 1.311, + 5.125, -0.201), \tag{42}$$

where $\hat{q} = \log_{10}(Q)$ and Σ_P is a spliced sigmoid function: Beginning with a standard sigmoidal function $\Sigma(x) = [\exp(x) - 1.0]/[\exp(x) + 1.0]$ that transitions between -1 and $+1$ as x transitions from large negative values to large positive values, a spliced form is constructed by joining two separate rescaled sigmoid representations at a transition point $x = D$ as

$$\Sigma_P(x, A, B_1, B_2, C_1, C_2, D) = \begin{cases} A + B_1\Sigma[C_1(x-D)], & x \leq D, \\ A + B_2\Sigma[C_2(x-D)], & x \geq D. \end{cases} \tag{43}$$

By requiring $B_1C_1 = B_2C_2$, both the value of the function and its slope will be contiguous at $x = D$. This function approximates the curve plotted in Fig. 2 of Ref. 5. The current form has been tailored for the range $-2 < \hat{q} < +2$.

The $G(Q)$ function is parameterized such that it models the main diffraction effects on the tilt-variance while the relative strength of the effect has been aggregated in the leading constant.

The addition of the central obscuration modulates Eq. (41) to the following form:

$$\langle \mathbf{a}\cdot\mathbf{a}\rangle = 2.0864\frac{J(S)}{D_2^2}\frac{[\mathcal{W}_1(C)-\mathcal{W}_3(C)]}{(0.0375-0.0049)}\tilde{G}(Q,C), \tag{44}$$

introducing functions $\mathcal{W}_1(C)$, $\mathcal{W}_3(C)$, and $\tilde{G}(Q,C)$. The form of this equation is organized such that the constants 0.0375 and 0.0049 reflect the limiting behaviors of the $\mathcal{G}$ functions as the influence of $\alpha(Qu)$ on the phase structure function D_ϕ [Eq. (4)] approaches its limiting value of 1 for large Q. The $\mathcal{W}$ reflect generalizations of these constants, given as

$$\mathcal{W}_1(C) = \frac{1}{(1-C^4)}\int_0^1 \mathcal{G}_1(u,C)u^{8/3}\mathrm{d}u \approx 0.0375 - 0.0110C^{2.25} + 0.0070C^{2.75}, \tag{45}$$

$$\mathcal{W}_3(C) = \frac{1}{(1-C^4)}\int_0^1 \mathcal{G}_3(u,C)u^{8/3}\mathrm{d}u \approx 0.0049 - 0.0055C^{1.85} + 0.0036C^{2.75}. \tag{46}$$

The third function, $\tilde{G}(Q,C)$, has been similarly formulated as $G(Q)$ so that it approaches a limiting value of unity for large Q but also reflects the influences of C. It can be expressed as a modulated version of the original $G(Q)$ function

$$\tilde{G}(Q,C) = \int_0^1 \frac{[\mathcal{G}_1(u,C)-\mathcal{G}_3(u,C)]}{(1-C^4)[\mathcal{W}_1(C)-\mathcal{W}_3(C)]}u^{8/3}\alpha(Qu)\mathrm{d}u \approx G[Q\times 10^{+X_A(C)}], \tag{47}$$

using the function

$$X_A(C) \approx +0.096C^{2.95}. \tag{48}$$

These functions all have relatively minimal impact [see, e.g., Figs. 6 through 8 of Ref. 16], which is consistent with the concept that tilt effects are dominated by low wavenumber turbulence, with wavelengths wider than the system aperture.

4 Annular Aperture Tilt-Phase Correlation Calculations

The remaining impact to be quantified from Eq. (11) is the influence of the TP correlation TP. But, in doing so, we recognize, based on Eqs. (24) and (46), that the TV term is independent of the integration variable $\mathbf{v}$ in Eq. (11), as is the wave structure function [first term in the exponential in Eq. (11)]. Therefore, these terms can be factored out of the integral. Conversely, the TP term is dependent on $\mathbf{v}$, and we must write

$$M_{\mathrm{TP}}(\omega) = \int \mathrm{d}\mathbf{u}\frac{\tilde{W}(\mathbf{u}+\boldsymbol{\omega}/2)\tilde{W}(\mathbf{u}-\boldsymbol{\omega}/2)}{[\pi(1-C^2)/4]M_0(\omega,C)} \times \exp\{+\mathrm{TP}(D_2\mathbf{u},\boldsymbol{\omega})\}, \tag{49}$$

where the aperture effect has been normalized such that the entrance pupil area can be written using $\tilde{A} = \pi(1-C^2)/4$. Integration variable $\mathbf{v}$ has also been replaced by $\mathbf{u} = \mathbf{v}/D_2$.

The full transition to a dimensionless form for TP requires several additional steps. Introducing $\mathbf{a} = W_T\mathbf{p}$ and the Eq. (30) definition of the components into Eq. (10), then using Eq. (10) in the remnants of $\mathcal{D}_\psi$ in Eq. (8) (gives us a 1/2 factor), and applying isotropic and homogeneous conditions for the structure functions

$$\begin{aligned}\mathrm{TP}(\mathbf{v},\boldsymbol{\omega}) &= \frac{2}{2}\langle[\phi(\mathbf{v})-\phi(\mathbf{v}-D_2\boldsymbol{\omega})][\mathbf{a}\cdot(D_2\boldsymbol{\omega})]\rangle \\ &= \left\langle[\phi(\mathbf{v})-\phi(\mathbf{v}-D_2\boldsymbol{\omega})]\left[D_2W_T^2\int \mathrm{d}\mathbf{v}'W(|\mathbf{v}'|)\phi(\mathbf{v}')(\mathbf{v}'\cdot\boldsymbol{\omega})\right]\right\rangle \\ &= \frac{D_2W_T^2}{2}\int \mathrm{d}\mathbf{v}'W(|\mathbf{v}'|)(\mathbf{v}'\cdot\boldsymbol{\omega})\langle 2\phi(\mathbf{v})\phi(\mathbf{v}')-2\phi(\mathbf{v}-D_2\boldsymbol{\omega})\phi(\mathbf{v}')\rangle \\ &= \frac{D_2W_T^2}{2}\int \mathrm{d}\mathbf{v}'W(|\mathbf{v}'|)(\mathbf{v}'\cdot\boldsymbol{\omega})[-\mathcal{D}_\phi(\mathbf{v}-\mathbf{v}')+\mathcal{D}_\phi(\mathbf{v}-\mathbf{v}'-D_2\boldsymbol{\omega})].\end{aligned} \tag{50}$$

Introducing dimensionless $\mathbf{u} = \mathbf{v}/D_2$ and rewriting the two phase structure function elements based on Eq. (4)'s decomposition into J and Y functions

$$\begin{aligned}\mathrm{TP} = \frac{D_2^4W_T^2J(S/Q)}{2}\int \mathrm{d}\mathbf{u}'\tilde{W}(|\mathbf{u}'|)(\mathbf{u}'\cdot\boldsymbol{\omega}) \\ \times\{Y[Q(\mathbf{u}-\mathbf{u}'-\boldsymbol{\omega})]-Y[Q(\mathbf{u}-\mathbf{u}')]\}.\end{aligned} \tag{51}$$

The resulting integral is now only a function of $\mathbf{u}$, Q, and C. We also use the normalized $\tilde{W}$ window function. The results of this integral can be tabulated and interpolated separately for a more general recombining with multiple values of the leading turbulence strength factor. The results are also independent of the vector nature of $\boldsymbol{\omega}$ due to rotational aperture symmetry. Thus, the tabulated results need only be five-dimensional, facilitated by assuming $\boldsymbol{\omega} = \omega\hat{\mathbf{x}}$ is oriented along the x-axis.

To evaluate the integral in Eq. (51), let us divide the window function $\tilde{W}$ into an inner and an outer portion using the form

$$\begin{aligned}F_X(Q,C,\mathbf{u},\omega) = \int \mathrm{d}\mathbf{u}'\mathrm{Cyl}\left[\frac{|\mathbf{u}'|}{C}\right](\mathbf{u}'\cdot\omega\hat{\mathbf{x}}) \\ \times[Y(Q|\mathbf{u}-\mathbf{u}'-\omega\hat{\mathbf{x}}|)-Y(Q|\mathbf{u}-\mathbf{u}'|)],\end{aligned} \tag{52}$$

such that

$$\mathrm{TP} = \frac{32J(S/Q)}{\pi(1-C^4)}[F_X(Q,1,\mathbf{u},\omega)-F_X(Q,C,\mathbf{u},\omega)]. \tag{53}$$

Finally, to evaluate M_{TP}, we use the following N-factor adjustment

$$\begin{aligned}M_{\mathrm{TP}}(\omega) = \exp(N)\int \mathrm{d}\mathbf{u}\frac{\tilde{W}(\mathbf{u}+\boldsymbol{\omega}/2)\tilde{W}(\mathbf{u}-\boldsymbol{\omega}/2)}{[\pi(1-C^2)/4]M_0(\omega,C)} \\ \times\exp\{+\mathrm{TP}(\mathbf{v},\boldsymbol{\omega})-N\},\end{aligned} \tag{54}$$

where variable N ensures that the integral can be evaluated within the numerical precision of the machine in the presence of large S (strong turbulence). Use of F_X means only two sets of tabulated results need to simultaneously reside in the computer memory to evaluate results for any given C value.

5 Combined Short-Exposure Atmospheric Modulation Transfer Function Model

Sections 3 and 4 developed expressions for the TV and TP components of SEMTF, respectively. Let us summarize these results here. The overall model of the short-exposure expression will be written as

$$\begin{aligned}M_S(\omega) &= M_0(\omega,C)M_{\mathrm{SA}}(\omega,S,Q,C) \\ &= M_0(\omega,C)M_{\mathrm{LA}}(\omega,S)M_{\mathrm{TV}}M_{\mathrm{TP}}.\end{aligned} \tag{55}$$

The M_0 expression is given in Eq. (21). M_{SA} is the complete short-exposure atmospheric MTF consisting of long-exposure (LA), TV, and TP components. The LA component can be written

$$M_{\mathrm{LA}}(\omega,S) = \exp\{-\mathcal{D}(D_2\omega)/2\} = \exp\{-J(S\omega)/2\}, \tag{56}$$

using the wave structure function from Eq. (3). The remaining two components are obtained from the M_{TV} component constructed from

$$\begin{aligned}M_{\mathrm{TV}}(\omega,S,Q) &= \exp(-\mathrm{TV}) \\ &= \exp\left\{-1.0432S^{5/3}\frac{[\mathcal{W}_1(C)-\mathcal{W}_3(C)]}{(0.0375-0.0049)}\tilde{G}(Q,C)\omega^2\right\},\end{aligned} \tag{57}$$

where the TV term in Eq. (11) has been expanded using Eq. (22) and $\langle\mathbf{a}\cdot\mathbf{a}\rangle$ from Eq. (44).

The remaining M_{TP} effect must be evaluated numerically using Eq. (54). However, rather than leave the results only in this tabulated format, an integrated short-exposure correction term has been developed as a perturbation of the original solution suggested by Fried in treating the circular case

$$M_{\mathrm{SA}}(\omega,S) = \exp\{-J(S\omega)/2[1-\tilde{\alpha}\omega^{1/3}]\}. \tag{58}$$

Here, Fried[15] recommended setting the $\tilde{\alpha}$ parameter to either a value of 0.5 or 1.0 (small and large Q cases). Here, the M_{TV} and M_{TP} effects are combined to replace Fried's $\tilde{\alpha}$ by the function $V(\omega,X,Q,C)$

$$\begin{aligned}M_{\mathrm{TP}}(\omega,S,Q,C)M_{\mathrm{TV}}(\omega,S,Q,C) \\ = \exp\{[J(S\omega)/2]V(\omega,2.1S,Q,C)\omega^{1/3}],\end{aligned} \tag{59}$$

where $X = 2.1S$ replaces S.

To tabulate these effects, function $V(\omega,X,Q,C)$ was evaluated at 103 ω values, 41 logarithmically increasing X values ranging from 0.1 to 10^3, 9 logarithmically increasing Q values ranging from 1/16 to 16, and 12 C values ranging from 0.00 to 0.95, for a total of 456,084 calculations.

To parameterize the C variability, a parameterized C dependence is constructed for each parameter

$$U(C) = U_0 + U_1C + U_2C^2 + U_3C^3 + U_4C^4 + U_5C^5. \tag{60}$$

The original circular aperture solution was handled as an 80-parameter model. Using the above expression, each of the 80 parameters would need to be characterized by six separate parameters, resulting in a 480-parameter model.

The forms taken by the V at different C values are plotted in a series of graphs below. Figure 4 illustrates samples from the original circular aperture data set. The two groups of lines

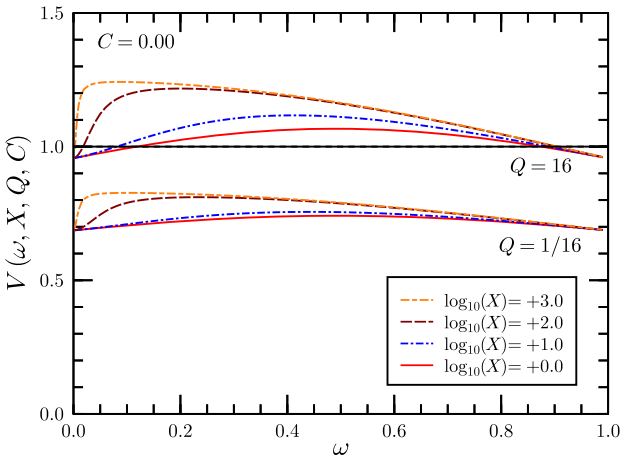

Fig. 4 Unnormalized $V(\omega, X, Q, C)$ for $C = 0.00$.

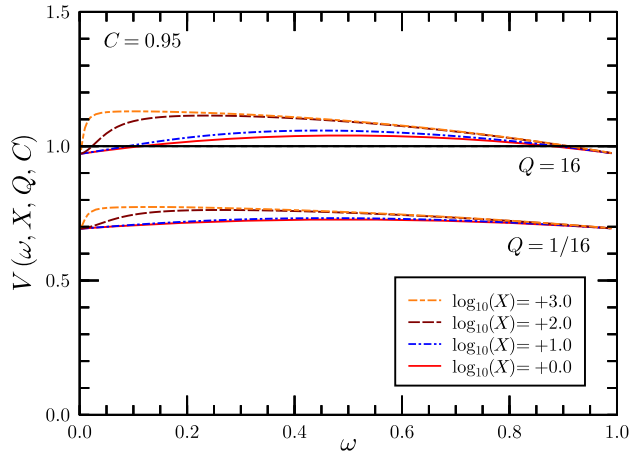

Fig. 6 Unnormalized $V(\omega, X, Q, C)$ for $C = 0.95$.

denote $Q = 1/16$ and $Q = 16$ behaviors at [essentially] the extents of low Q (high diffraction effects) and high Q (far-field) imaging conditions. (Telescope type systems typically operate in the range of $Q = 2 \ldots 4$.) One finds that the behavior of V does not change significantly above $Q = 2$.

The significant feature of the V curves at high Q values is that they exceed unity over a range of frequencies ω but fall below unity as $\omega \to 1$. By falling below 1.0 at high frequency, the resulting forms obey diffraction limits, as expected. Conversely, when $V > 1$ at intermediate frequencies, one sees a midrange frequency correction of long-exposure turbulence blurring. This recovery is limited to high Q system configurations.

Extending the results illustrated in Fig. 4 to noncircular apertures, Figs. 5 and 6 illustrate behaviors under conditions of moderate ($C = 0.50$) and large ($C = 0.95$) obstructions. As shown, the main impact of increasing central obscuration is to affect midrange spatial frequencies. V values at these frequencies become increasingly attenuated as C increases. Nonetheless, interestingly, the floor values of the functions (at $\omega = 0$ and $\omega = 1$ frequencies) remain unaffected.

To more directly compare these results, Fig. 7 shows V values from a moderately strong turbulence scenario ($X = 10$) for a moderately large aperture ($Q = 4$) over a range of C parameter values. Here, C varies from 0.00 to

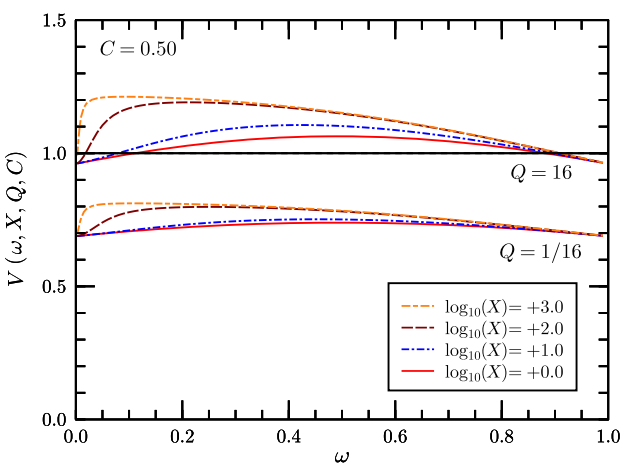

Fig. 5 Unnormalized $V(\omega, X, Q, C)$ for $C = 0.50$.

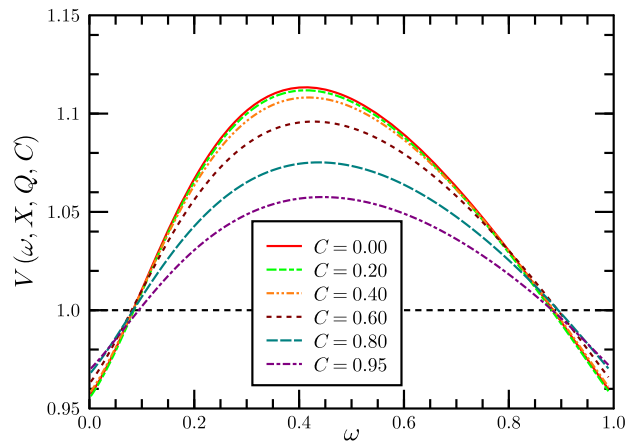

Fig. 7 Plots of $V(\omega, X, Q, C)$ for varying central obscuration parameter C for $Q = 4$ and $X = 10$.

0.95, but most of the dynamic effects (degradation of the MTF in the high C range) are not significant before $C = 0.30$ and are only severe beyond $C = 0.50$. Thus, the majority of systems operating at $C \leq 0.50$ experience turbulence effects nearly identical to that of circular apertures, differing primarily in terms of the form of the system MTF.

To further examine the variability of the V function, let us next note from a comparison of Figs. 5 and 6 how similar the evolution of a given family of V curves is for a given Q and C combination as X (S) and ω are varied. The primary elements that appear to change dramatically are the height of the baseline value of V along with the height of the peak above the baseline. The former is termed $V_0(Q, C)$, and the latter is designated as $V_M(Q, C)$. Figures 8 and 9 illustrate these functional behaviors.

As illustrated in Fig. 8, there are minimal differences in V_0 as C varies. The primary driving factor appears to be due to diffraction, as parameterized by its Q variations.

The V_M function appears to exhibit both variations in C and Q. As opposed to the V_0 function, the influence of the central obscuration can significantly modulate this height. Note, particularly, that increasing C has a degrading effect on the midrange frequency enhancement noted for the circular aperture case. Nonetheless, we find that for relatively

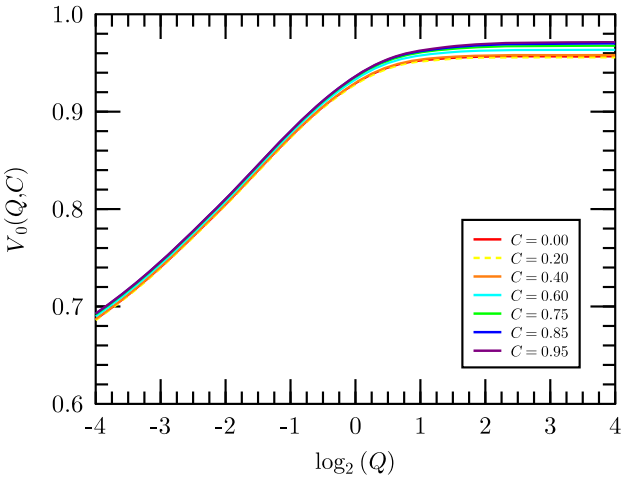

Fig. 8 Plots of minimum $V(\omega, X, Q, C)$ values (V_0) as functions of increasing Q for different aperture central obscuration fractional widths C.

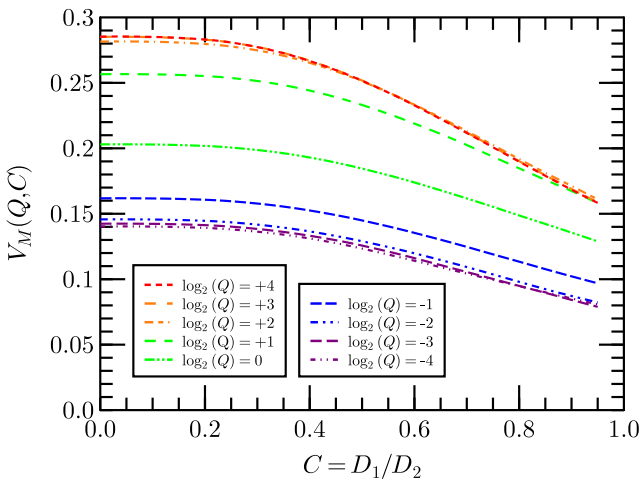

Fig. 9 Plots of difference between the maximum $V(\omega, X, Q, C)$ values (captured from the $X = 1000$ results) above the minimum V values (V_0) for various Q and C combinations.

large apertures ($Q > 2$), there is in fact no value of C that will not produce the needed enhancement to result in $V > 1$ at some range of frequencies. On the other hand, if Q is small, e.g., $Q < 1/16$, there is no C value that can produce the frequency enhancement region. Also, we see again that for $C < 0.3$ and $Q > 2$ one finds a plateau region where the behavior of the annular system approximates that of the circular aperture system.

6 Applicability

Dashen's[11] analysis of the applicability of the RA is now reviewed. Dashen proposed two parameters, Φ and Θ, to describe the influences of diffraction and turbulence on the propagation environment. According to Dashen, if $\Theta \gg \Phi$ the RA should apply, where Φ represents the rms phase fluctuation using first-order geometric optics to measure turbulence effects and Θ represents the diffraction effects due to a characteristic scale size of the turbulence itself. These two parameters were studied in Ref. 6, resulting in the relation

$$\Phi = \sqrt{2.31k^2 L C_n^2 L_o^{5/3}} = 3.815(L_o/r_0)^{5/6}, \tag{61}$$

using the relation for r_0 in Sec. 2.1 and where L_o is the turbulence outer scale, and

$$\Theta = 6k\Lambda^2/L = 716.6L_o^2/F^2, \tag{62}$$

using the Fresnel zone, $F = (\lambda L)^{1/2}$, and $\Lambda = 4.36L_o$. (This result represents the peak of the turbulent spectrum, essentially the integral scale.)

Taking the ratio

$$\frac{\Theta}{\Phi} = 187.8\frac{L_o^{7/6} r_0^{5/6}}{\lambda L} = \frac{75.038 L_o^{7/6}}{L^{3/2}(C_n^2)^{1/2}} \gg 1. \tag{63}$$

Using typical values, this condition is easily achieved (e.g., $L_o \geq 0.5$ m, $C_n^2 < 10^{-12}$ m$^{-2/3}$, $L \leq 10$ km). Potvin[17] has further shown recently that RA is consistent with beam steering based on Fermat rays (the Eikonal) affected by large-scale turbulent perturbations.

Moreover, from this author's perspective, the RA is under-rated, often being conflated with the Born approximation. The alternative, the mutual coherence function (MCF) approach, measures the degree to which an advancing wavefront loses coherence. Incoherent light involves the propagation of individual decorrelated photons. It is difficult to imagine how any given photon could become decorrelated from itself. Hence, MCF does not appear to be examining the same problem, and it may be that the RA is closer to the correct approach for handling incoherent radiation.

7 Conclusions

The complete model of the annular aperture SEMTF involves 480 parameter values consistent with the 80-parameter circular aperture model expanded to the annular aperture through use of the polynomial construction of Eq. (61), which multiplies the total number of parameters by a factor of six. The full model is available upon request and approval through appropriate channels.

In light of the degrading behavior of the SEMTF as C increases, one wonders whether additional terms that would significantly improve the performance could be relatively easily introduced. Hufnagel[18] addressed higher order phase corrections, but only for circular apertures. Perhaps the full annular aperture problem could supply added correction capabilities at high turbulence levels that are not achievable for circular apertures.

The development and analysis process described have been designed to provide system modelers and developers a tool for simulating a broad spectrum of system conditions and behaviors. In general, the behavior of annular aperture systems do not deviate significantly from circular aperture systems until $C > 0.4$. Study results may also be of use to adaptive optics designers by providing a baseline of performance when no correction is applied.

References

1. G. C. Holst, *Electro-Optical Imaging System Performance*, 3rd ed., SPIE Press, Bellingham, Washington (2002).
2. K. Krapels et al., "Atmospheric turbulence modulation transfer function for infrared target acquisition modeling," *Opt. Eng.* **40**, 1906–1913 (2001).

3. N. S. Kopeika, *A System Engineering Approach to Imaging*, SPIE Press, Bellingham, Washington (1998).
4. D. L. Fried, "Optical resolution through a randomly inhomogeneous medium for very long and very short exposures," *J. Opt. Soc. Am.* **56**(10), 1372–1379 (1966).
5. D. H. Tofsted, "Reanalysis of turbulence effects on short-exposure passive imaging," *Opt. Eng.* **50**(1), 016001 (2011).
6. D. H. Tofsted, "Extended high-angular-frequency analysis of turbulence effects on short-exposure imaging," *Opt. Eng.* **53**(4), 044112 (2014).
7. D. H. Tofsted, "Short exposure passive imaging through path-varying convective boundary layer turbulence," *Proc. SPIE* **8355**, 83550J (2012).
8. V. N. Mahajan and B. K. C. Lum, "Imaging through atmospheric turbulence with annular pupils," *Appl. Opt.* **20**(18), 3233–3237 (1981).
9. G.-M. Dai and V. N. Mahajan, "Zernike annular polynomials and atmospheric turbulence," *J. Opt. Soc. Am. A* **24**(1), 139–155 (2007).
10. M. I. Charnotskii, "Anisoplanatic short-exposure imaging in turbulence," *J. Opt. Soc. Am. A* **10**(3), 492–501 (1993).
11. R. Dashen, "Path integrals for waves in random media," *J. Math. Phys.* **20**(5), 894–920 (1979).
12. J. W. Goodman, *Statistical Optics*, John Wiley & Sons, New York (1985).
13. R. S. Lawrence and J. W. Strohbehn, "A survey of clear-air propagation effects relevant to optical communications," *Proc. IEEE* **58**(10), 1523–1545 (1970).
14. J. D. Gaskill, *Fourier Optics*, John Wiley & Sons, New York (1978).
15. D. L. Fried, "Statistics of a geometric representation of wavefront distortion," *J. Opt. Soc. Am.* **55**(11), 1427–1435 (1965).
16. D. H. Tofsted, "Modeling optical turbulence effects on centrally obscured aperture systems," *U. S. Army Research Laboratory*, ARL-TR-6273, White Sands Missile Range, New Mexico (2012).
17. G. Potvin, "General Rytov approximation," *J. Opt. Soc. Am. A* **32**(10), 1848–1856 (2015).
18. R. E. Hufnagel, "The probability of a lucky exposure," Technical Memorandum REH-0155, Perkin-Elmer (1989).

David H. Tofsted is a physicist with the U.S. Army Research Laboratory at White Sands Missile Range, New Mexico, with over 36 years in service. He received his BS degree in physics from Pennsylvania State University in 1979 and his MS degree and PhD in electrical engineering from New Mexico State University, New Mexico, in 1992 and 2013, respectively. His research has focused on optical propagation problems impacted by atmospheric effects. His work includes numerical simulations of optical turbulence, sensing and predicting turbulence strength, and mitigation methods. He has authored over 60 publications.